AIAA Aviation 2022 Forum, 27 June - 1 July 2022, Chicago, IL, Article number AIAA 2022-3619
DOI: 10.2514/6.2022-3619

Risk-based Flight Planning and Management for Urban Air Mobility

Yu Su* and Yan Xu†
Cranfield University, Bedford, MK43 0AL, United Kingdom

This paper investigates a quantitative ground risk assessment method for future urban air mobility, which can be divided into three main processes: risk modelling, risk assessment and mitigation recommendation for flight planning and management. First, the aircraft kinetic models for both fixed-wing aircraft and rotorcraft are investigated, along with the corresponding ballistic and glide descent mode and the associated wind influence. The probabilistic impact to road traffic and pedestrians on the ground as a result of potential crash are then derived. With an assumed crash probability of the aircraft, the initial risk value and distribution are computed, which are used to produce a risk cost map across the mission area. Next, the flight request is processed based on such risk map using a common path planning algorithm, minimizing the overall risk for the flight plan to be generated. Finally, a preliminary case study involving a rotorcraft conducting urban cargo transportation service is performed to evaluate the proposed risk assessment method in a real-world urban environment.

I. Introduction

With the technological development of electric vertical take-off and landing (e-VTOL) vehicles and unmanned aircraft systems (UAS), future urban air mobility (UAM) has become a research area of widespread interests. Nowadays, land resources needed for ground transportation cannot substantially increase with the population expansion and the traffic demand in megacities. The development of UAM is a promising solution for the future urban transportation system. The small UAS and general aviation (manned aircraft) already being used for various purposes in urban environments, such as traffic monitoring [1], are also a core component of UAM [2] which forms a part of the plans for smart cities in the near future [3, 4].

UAM enables highly automated, cooperative, passenger or cargo-carrying air transportation services in and around urban areas. In the popularization of UAM, integrating UAM into urban and suburban airspace is challenging, as it entails risks from a safety perspective. When producing coverage for outdoor events in typical urban and suburban scenarios, UAM face relevant risks including collisions with ground buildings, traffic routes, and pedestrians. The Joint Authorities for Rulemaking on Unmanned Systems (JARUS) pursues a consensus from various National Aviation Authorities (NAAs) and stakeholders on a common procedure to identify and qualitatively assess safety risks for Unmanned Aircraft System (UAS) operations [5]. JARUS has developed the Specific Operational Risk Assessment (SORA), which is a novel approach on how to safely create, evaluate and conduct an UAS operation [6]. It focuses on assigning to an UAS-operation two classes of risk, a ground risk class (GRC) and an air risk class (ARC). SORA allows operators to utilise certain mitigating measures to reduce both risk-classes [7, 8].

In addition to SORA, scholars have also conducted in-depth discussions on the risk assessment methods for UAM from different aspects, resulting to a series of risk assessment methods for some specific scenarios. Ref [9–11] proposed the concept of risk cost map that associates discretized locations of the space with a suitable risk cost. Ref [12] proposed models for risk assessment of UAS operations over road networks. Going further, they investigated the feasibility of a long-range inspection mission of railways by UAS from a risk point of view [13]. Ref [14] presented a risk evaluation method to measure the risk of UAS to urban ground buildings. Besides, a risk model was established to quantitatively analyze the risk caused by UAS to ground buildings. Ref [15] analyzed the safety threat caused by UAS to ground pedestrian and conducted risk modelling. The evaluation criteria was introduced, based on the defined risk cost calculation indicators, leading to the generation of the UAS operation risk map.

In order to accurately predict the magnitude and distribution of the risk that UAM may cause to the ground before the mission is executed, this paper proposes a quantitative ground risk assessment method to generate a pre-flight risk cost map. With this approach, the UAM operator will know the risk distribution for the mission airspace without a

*PhD candidate, School of Aerospace, Transport and Manufacturing, B105 DARTeC, Cranfield University, AIAA Student Member.
†Lecturer in ATM/CNS, School of Aerospace, Transport and Manufacturing, B105 DARTeC, Cranfield University, AIAA Member.

Published by AIAA. This is the Author Accepted Manuscript issued with: Creative Commons Attribution Non-Commercial License (CC:BY:NC 4.0).
The final published version (version of record) is available online at DOI:10.2514/6.2022-3619. Please refer to any applicable publisher terms of use.

specific flight plan, and thus avoid high-risk areas when generating a flight plan in such a way to improve flight safety. To evaluate the proposed risk assessment framework, we simulate a specific scenario aimed at a real world urban area, with a use case of cargo transportation using a quadcopter. The ground (road traffic and pedestrian) risk is assessed and a low-risk flight plan is produced on the generated risk cost map.

The remainder of this paper is organized as follows: section 2 motivates our position based on gaps and inconsistencies we have identified in SORA, and also introduces the structure of our proposed risk assessment framework for UAM; in section 3, we introduce the risk modelling steps for different types of aircraft in the risk assessment model; section 4 uses the risk assessment model to analyze the road traffic and pedestrian risk in a real urban area, and uses the obtained risk cost map combined with the path planning algorithm to obtain a low-risk flight plan; section 6 summarizes the work of this paper and gives an outlook of future work.

II. Research motivation

Application and analysis showed that the SORA process is far from being finished. The GRC/ARC lookup table is based on a simple scoring. While overall the scoring seems to have a logical background, proof on why the scores are the way they are is missing. JARUS refers to annex G of the SORA guidelines that shall include supporting theories; this annex has not yet been released. In the operating environment of UAM, air traffic participants are not only UAS, but also manned aircraft, eVTOL and so on. If only the risk division method of SORA is used, the differences in the structure of different aircraft, the differences in flight performance, and the differences in accident risk caused by mission differences will be ignored. Furthermore, risk level lookup tables alone do not reflect the distribution of risk in mission airspace.

Leveraging on a thorough analysis of the current state-of-the-art in UAM, a high-level ConOps was proposed in the AMU-LED project [16] to accommodate UAM within the existing U-space vision to cover the particularities of the specific UAM users, missions, stakeholders and business cases while tackling the main challenges that are specific to urban scenarios. This ConOps targets a mid-term scenario (2025-2030) when the first so-called High-Performing operations (i.e. air-taxi and cargo) will start taking place within a relatively mature U-space environment with most U1 and U2 services deployed in cities. To guarantee safety and efficiency in this mid-term scenario where operations are not yet fully integrated, the ConOps proposes to set up an intermediate layer containing these high-performing vehicles (HPVs), high-risk traffic below the Very Low Level to segregate it from manned aviation operating above. Similarly, these operations will be segregated from other less performing, less-risk unmanned vehicles, i.e., standard-performing vehicles (SPVs), operating in the lowest airspace and subject to less restricting requirements.

To sum up, in the face of the urban operation scenario of UAM, it is necessary to develop a comprehensive risk assessment method, which considers the flight (HPV/SPV) performance parameters of different air traffic participants, air and ground environmental factors, quantifies the specific risk distribution in the mission area, and generates a risk distribution map. Risk distribution maps will play a key role in guiding the generation of pre-mission flight plans for UAM operations in cities. Existing SORA methods follows a qualitative way in the assessment of risk. This paper proposes a more detailed quantitative risk assessment method for UAM. The basic structure of the risk assessment model proposed in this paper is shown in Figure 1. The entire risk assessment framework is divided into three parts: risk modelling, risk assessment and mitigation recommendation. Firstly, the aircraft kinetic model is established using the known aircraft parameters, from which the mission expectations and the environment information of the task area are derived. All the above information will be processed in the risk assessment. In this step, parameters such as impact kinetic energy and crash probability of the aircraft will be calculated as preliminary risk assessment data. These data will superimpose influencing factors such as weights and masking parameters to obtain the final risk value to road traffic and pedestrians on the ground. The results of risk assessment will be fused in the form of risk cost distribution map. Finally, the mitigation recommendation step combines risk cost maps and path planning algorithms to generate low-risk flight plans.

III. Risk assessment modelling

A. Definition and evaluation of risk

As introduced in Ref [17], there are usually a sequence of three conditional processes that a crash incident will cause fatality to road traffic or pedestrians: failure of UAM; falling UAM's impact to ground objects; and fatality damage caused to vehicles or pedestrians on the ground. Based on the above three processes, the risk value of UAM flying over a specific area is defined in this paper as the probability of fatalities per flight hour. The risk value is calculated as in

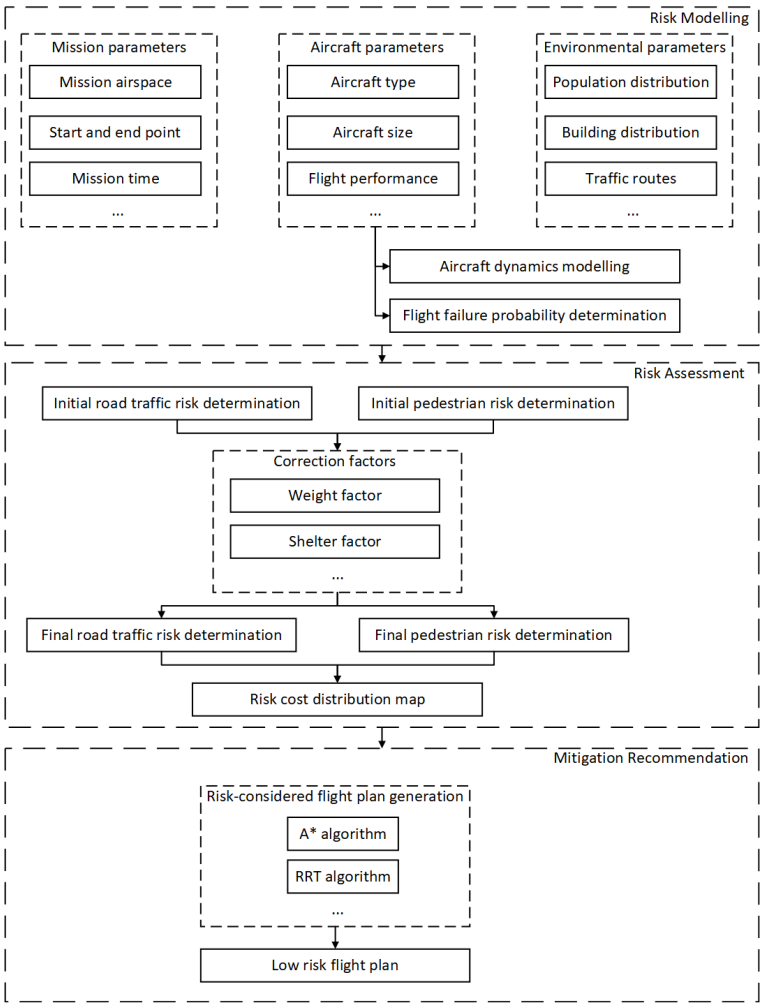


Fig. 1 Structure of the risk assessment approach used in this study.

Equation 1, where R is the risk value, P_{crash} is the probability of UAM failure, P_{impact} is the probability to impact an object due to the falling UAM, which is a function of the number of vehicles or pedestrians on the ground, $P_{fatality}$ is the fatality rate, which is mainly associated to the function of kinetic energy.

$$R = P_{crash} \cdot P_{impact} \cdot P_{fatality} \tag{1}$$

For the probability of an UAM crash P_{crash}, in the urban low-altitude airspace environment, there could co-exist various new types of aircraft which leads to a complicated situation for identifying the crash probability. Traditional aviation historical data cannot be directly used to estimate such probability. According to the AMU-LED ConOps introduced in Sec. II, the main UAM participants may include conventional manned aircraft (such as helicopter), high performance vehicle HPV (such as urban air taxis), and standard performance vehicle SPV (such as delivery drone and aerial photography drone). Considering that UAM contains different types of participants, the following UAM participants are collectively referred to as aircraft, and aircraft is divided into fixed-wing aircraft and rotary-wing aircraft type. The probability of an aircraft crash quantifies the frequency associated with the aircraft accident. Usually, it is consistent with the failure rate of the aircraft system, expressed in flight hours. Referring to [18], the commercial manned aircraft failure rate is set at $1/10^5$ flight hours, and HPV is assumed at $1/10^4$ flight hours, while $1/10^3$ flight hours for SPV in this paper.

Next, we need to estimate P_{impact} as a function of the number of vehicles or pedestrians hit by a falling aircraft. This requires to model the falling process of aircraft. In [19], Harbo et al. considered four different types of uncontrolled descent of an aircraft: ballistic descent, uncontrolled glide, parachute descent and flyaway. According to the falling

characteristics of fixed wing aircraft and rotorcraft, the first two types of descent have been applied in this paper. The latter two models will be introduced in the future when considering the falling situation of the aircraft carrying a parachute and the aircraft out of control with power, which is beyond the scope of this paper.

Specifically, ballistic descent is a situation where the aircraft has lost most of its lift. The aircraft will then enter a (close to) ballistic descent governed solely by the aerodynamics of the aircraft. For the falling process of the rotorcraft, it can be regarded as a ballistic descent. For a fixed wing aircraft losing its thrust as well as losing power for the flight control surfaces, it may enter an uncontrolled gliding state. It is assumed that the aircraft wing structure is intact and that each control surface is close to the neutral position. The aircraft will enter a descent path governed by the glide ratio. According to the above characteristics, this paper will analyze the falling process of fixed-wing aircraft and rotorcraft respectively. By analyzing the force and motion trajectory of the falling process, the kinetic energy of the aircraft falling to the ground and the farthest falling range will be estimated.

The fatality rate $P_{fatality}$ is associated with two main factors: impact kinetic energy E_k and shelter factor $c_{shelter}$. The shelter factor defines the shelter level of the map. The shelter factor is a positive number used to quantify the shelter level of people in the area. This is critical in the sense that the presence of buildings and other obstacles in the aircraft crash area can reduce the kinetic energy at the time of impact, thereby reducing the probability of fatality. If shelter factors are not evaluated, the resulting risks may be too conservative, especially in the urban environment where buildings, vehicles, and trees protect the population. The fatality rate $P_{fatality}$ can be described by Equation 2, where α is the impact energy that might cause 50% fatality with $c_{shelter}$=0.5; β is the impact energy threshold required to cause fatality as $c_{shelter}$ approaching zero [20]. In this paper, we set α to 10^6 J and β to 100 J.

$$P_{fatality} = \frac{1}{1 + \sqrt{\frac{\alpha}{\beta}} \left(\frac{\beta}{E_k}\right)^{\frac{1}{4c_{shelter}}}} \tag{2}$$

Aircraft kinetic energy E_k can be expressed by the following equation:

$$E_k = \frac{mv^2}{2} \tag{3}$$

where the aircraft mass m is known and the speed of the aircraft hitting the ground v needs to be predicted, as follows:

$$v^2 - v_0^2 = 2ax \tag{4}$$

$$v = v_0 + at \tag{5}$$

Aircraft acceleration a:

$$a = \frac{F}{m} \tag{6}$$

The gravity of the aircraft $F_{gravity}$:

$$F_{gravity} = mg \tag{7}$$

Aircraft drag $F_{resistance}$ estimation:

$$F_{resistance} = \frac{\rho v^2 C_D A}{2} \tag{8}$$

where C_D is the drag coefficient, and A is the windward area of the aircraft.

B. Analysis of the descent process

With the above definition of risk, we first estimate P_{impact} which is assumed to be linearly correlated to the number of affected vehicles/pedestrians N as a result of the crash, and then we estimate the subsequent fatality rate $P_{fatality}$. This requires the analysis of the falling process of the aircraft, evaluating the horizontal distance of the aircraft from failure to crash, as well as the kinetic energy when it collides with the ground. For aircraft with different structures, the falling characteristics are different. This paper analyzes the falling process of rotorcraft and fixed-wing aircraft respectively.

1. Analysis of the descent of rotorcraft

During the falling of the rotorcraft, the force on it can be expressed by the following equation:

$$\vec{F} = \vec{F}_{gravity} + \vec{F}_{thrust} + \vec{F}_{resistance} \tag{9}$$

According to Eq (8), C_D is the drag coefficient, and A is the projected area above the aircraft. Then the vertical acceleration a_y of aircraft is:

$$a_y = \frac{mg - F_{resistance}}{m} = g - \frac{\rho v_y^2 C_D A}{2m} \tag{10}$$

According to Eq (5), the vertical velocity when hitting the ground v_{yhit} from specified height H is:

$$v_{yhit} = \int_0^t g - \frac{\rho v_y^2 C_D A}{2m} dt = \sqrt{\frac{2mg}{\rho C_D A}\left(1 - e^{-\frac{\rho C_D A H}{m}}\right)} \tag{11}$$

Since the forward wind resistance area of the rotorcraft is small, the horizontal forward resistance is ignored. The cruising speed of the aircraft is v_{cruise} approximately equal to the horizontal velocity v_{xhit}. The impact kinetic energy E_k of the rotorcraft on the ground is:

$$E_k = \frac{mv_{xhit}^2}{2} + \frac{mv_{yhit}^2}{2} = \frac{mv_{cruise}^2}{2} + \frac{m^2 g}{\rho C_D A}\left(1 - e^{-\frac{\rho C_D A H}{m}}\right) \tag{12}$$

The time it takes for the aircraft to fall from height h to the ground is t_{fall}, The relationship between fall time t_{fall} and flying height h is shown in the following equation:

$$t_{fall} = \sqrt{\frac{2m}{\rho C_D A g}} \cosh^{-1}\left(e^{\frac{\rho C_D A H}{2m}}\right) \tag{13}$$

Then for the rotorcraft, the horizontal threatening distance L_{threat} when the fault occurs is:

$$L_{threat} = v_x \cdot t_{fall} = v_{cruise}\sqrt{\frac{2m}{\rho C_D A g}} \cosh^{-1}\left(e^{\frac{\rho C_D A H}{2m}}\right) \tag{14}$$

2. Analysis of the descent of fixed-wing aircraft

During the falling of the fixed-wing aircraft, the force on it can be expressed by the following equation.

$$\vec{F} = \vec{F}_{lift} + \vec{F}_{gravity} + \vec{F}_{thrust} + \vec{F}_{resistance} \tag{15}$$

Aircraft lift:

$$F_{lift} = \frac{C_y \rho v^2 S}{2} \tag{16}$$

where C_y is the lift coefficient, ρ is the air density, S is the wing area. When the power fails, the aircraft can be regarded as a glider, and the lift-to-drag ratio is equal to the glide ratio:

$$S_{lift} = K = \frac{F_{lift}}{F_{resistance}} = \frac{L}{H} \tag{17}$$

Among them, S_{lift} is the lift-to-drag ratio, K is the glide ratio, L_{threat} is the dangerous range of fixed-wing aircraft failure, and H is the flight altitude. Fixed-wing aircraft failure hazard range L_{threat}:

$$L_{threat} = HK = \frac{HF_{lift}}{F_{resistance}} \tag{18}$$

$$L_{threat} = H \cdot \frac{C_y \rho v^2 S}{2} \cdot \frac{2}{\rho v^2 C_D A} = \frac{HC_y S}{C_D A} \tag{19}$$

According to [19], ignoring the complex force and speed changes when gliding without power, and simplifying the process to a uniform falling motion, the horizontal speed is defined as the gliding speed and remains unchanged. The kinetic energy of the gliding state on the ground impact is calculated by the horizontal gliding speed. The impact kinetic energy E_k when the fixed-wing aircraft falls to the ground is shown below, and v_{glide} is the glide speed of the aircraft.

$$E_k = \frac{m v_{glide}^2}{2} \tag{20}$$

The descent time of the fixed-wing aircraft t_{fall} can be estimated by the following equation:

$$t_{fall} = \frac{L_{threat}}{v_{glide}} = \frac{H C_y S}{C_D A v_{glide}} \tag{21}$$

C. Wind influence

The effect of wind will affect the falling process of aircraft, thus affecting the risk distribution. For this, wind needs to be incorporated into the risk assessment system. In practice, existing research works mainly consider the impact of wind on flight risk in two ways: weather forecast for pre-flight phase or real-time wind information for in-flight phase.

In Ref [19], some information about wind direction and magnitude is first obtained at the pre-flight phase. In this case, the authors deal with the uncertainty in a stochastic manner during the evaluation of the location affected by the falling impact, choosing a two-dimensional parameterization of the wind and the associated assumptions of the probability distribution, normal distribution for wind magnitude and uniform distribution for wind heading angle. However, there may be huge uncertainties in the actual wind conditions faced by the aircraft during the in-flight phase. Thus, another method is to have real-time information of wind conditions during the flight. In [21], wind information achieved by using ad-hoc sensors along with estimation algorithms, therefore no statistical assumption will be taken.

In this paper, we combine the above two methods, the estimation of the wind condition ahead of flight, and the evaluation methods of real-time monitoring of wind direction and wind speed by sensors during flight. Before the mission, the wind information prediction is obtained through the weather forecast of the mission airspace, and the preliminary ground risk assessment is performed to generate a pre-flight risk cost map. During the flight mission, real-time wind change data can also be received, and the risk cost map will be corrected in real time.

Taking into account the effect of wind, the risk distribution will shift as a whole with the wind direction. The resistance F_{wind} received by the aircraft in the wind is shown in the following equation. In order to simplify the evaluation process, it is assumed that the windward area of the aircraft in all directions of the horizontal plane is approximately equal, which is $A_{horizontal}$, and v_{wind} represents wind speed.

$$F_{wind} = \frac{\rho v_{wind}^2 C_D A_{horizontal}}{2} \tag{22}$$

The wind deflection direction is opposite to the real-time wind direction, and distance $W_{distance}$ can be estimated by the following equation:

$$W_{distance} = \frac{a_x t_{fall}^2}{2} = \begin{cases} \dfrac{v_{wind}^2 A_{horizontal}}{2Ag} \cdot [\cosh^{-1}\left(e^{\frac{\rho C_D A H}{2m}}\right)]^2, & (rotorcraft), \\ \dfrac{\rho v_{wind}^2 A_{horizontal} H^2 C_y^2 S^2}{4 m C_D A^2 v_{glide}^2}, & (aircraft). \end{cases} \tag{23}$$

D. Risk assessment description

Equation 1 defines how the risk is calculated. Using this definition, we model the risk assessment for road traffic and pedestrians respectively.

1. Risk assessment for road traffic

The risk value of the aircraft to the road traffic is not only related to the impact kinetic energy of the aircraft itself hitting the ground, but also related to the speed, density of vehicles on the road and aircraft crash probability. Equation 24 is the estimation of the risk cost value R_{road} of the aircraft to the ground road. In order to control the magnitude of the risk cost for merging different aspects, w_{road} is considered as a weighted coefficient.

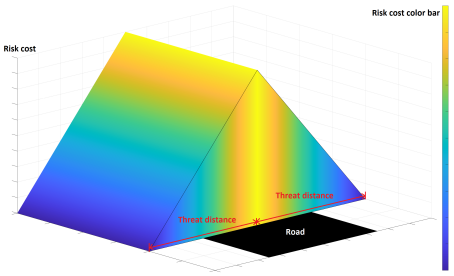


Fig. 2 Schematic diagram of the risk distribution of road traffic.

$$R_{road} = w_{road} \cdot P_{carimpact} \cdot P_{carfatality} \cdot P_{crash} \tag{24}$$

$P_{carimpact}$ is a linear function to the number of affected vehicles N_{car} which can be defined by equation 25. ρ_{car} is the road traffic density.

$$N_{car} = 2 \cdot L_{threat} \cdot \rho_{car} \tag{25}$$

$P_{carfatality}$ is the aircraft fatality rate to road traffic, which can be defined by equation 26.

$$P_{carfatality} = \frac{1}{1 + \sqrt{\frac{\alpha}{\beta}} \left(\frac{\beta}{E_{kcar}} \right)^{\frac{1}{4c_{shelter}}}} \tag{26}$$

E_{kcar} is the kinetic energy of the aircraft impacting the vehicle, as shown in equation 27. Impact kinetic energy takes into account the relative speed of the aircraft and ground vehicle. v_{car} is the road speed limit.

$$E_{kcar} = \frac{m(v_{xhit} + v_{car})^2}{2} + \frac{m v_{yhit}^2}{2} \tag{27}$$

The final road risk cost distribution map obtained according to the above risk assessment model is shown in Figure 2. As the figure shows, the risk value of the central area of the road is the highest, which is the risk cost R_{road} calculated by the Equation 24. From the centre of the road to the risk distance L_{threat}, the risk cost decreases linearly to zero.

2. Risk assessment for pedestrians

In addition to considering the risks to ground roads during aircraft operations, another important consideration on the ground is pedestrians. In order to more accurately assess the risk of UAM to pedestrians on the ground, it is necessary to assess the population distribution and the shelter factor of buildings and trees on the ground. Therefore, we use Multidimensional Open Data of Urban Morphology (MODUM) method to classify the study area. The study area is divided into the following types according to different functions: Suburban Landscapes, Railway Buzz, The Old Town, Victorian Terraces, Waterside Settings, Countryside Sceneries, High Street and Promenades and Central Business District.

Equation 28 is the estimation of the risk cost value R_{people} of the aircraft to the pedestrians. In order to control the magnitude of the risk cost, w_{people} is a weighted coefficient.

$$R_{people} = w_{people} \cdot P_{peopleimpact} \cdot P_{peoplefatality} \cdot P_{crash} \tag{28}$$

$P_{peopleimpact}$ is a linear function to the number of affected pedestrians N_{people} which can be defined by equation 29. ρ_{people} is the people density.

$$N_{people} = A_{fixwing/rotorcraft} \cdot \rho_{people} \tag{29}$$

First, we evaluate the impact area $A_{fixwing/rotorcraft}$ of fixed-wing aircraft and rotorcraft when they fall to the ground according to their flight characteristics. The expression used to compute the affected area for people in the open was given by the following equation. This expression has been previously introduced in Ref [22] and Ref [23].

$$A_{fixwing} = (w_{span} + 2R_p)(L_{aircraft} + \frac{H_p}{tan\gamma} + 2R_p) \tag{30}$$

For rotorcraft, the affected area can be expressed by the following equation.

$$A_{rotorcraft} = \pi \left(L_{aircraft} + \frac{H_p}{tan\gamma} + 2R_p \right)^2 \tag{31}$$

where $A_{fixwing}$ and $A_{rotorcraft}$ represents the estimated area affected by pedestrians on the ground after the fixed-wing and rotor aircraft falls. $L_{aircraft}$ is the farthest shape distance of the aircraft, H_p is the height of a person, for a standing pedestrian, defined as 1.75m. R_p is the radius of a person, defined as 0.25m. γ is the aircraft fall angle without power, the calculation method is shown in the following equation.

$$\gamma = \begin{cases} \tan^{-1}\left(\dfrac{C_y}{C_D}\right), & (aircraft), \\ \tan^{-1}\left(\dfrac{H}{v_{cruise}\sqrt{\dfrac{2m}{\rho C_D A g}}\cosh^{-1}\left(e^{\frac{\rho C_D A H}{2m}}\right)}\right), & (rotorcraft). \end{cases} \tag{32}$$

Figure 3 shows a schematic diagram of the estimated length of the rectangular area affected by the fall of a fixed-wing aircraft and Figure 4 shows the width of the rectangular area affected by the fall of a fixed-wing aircraft. Considering that the rotorcraft can fly toward any direction, the affected area is a circle with the aircraft as the center, and the radius is estimated as shown in Figure 5.

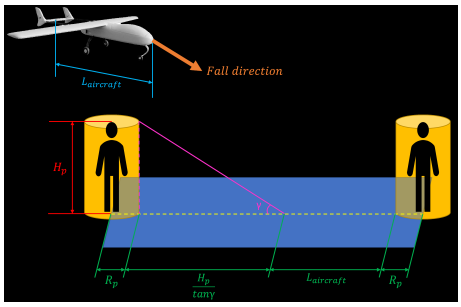


Fig. 3 Length of the area affected by the fall of the fixed-wing aircraft.

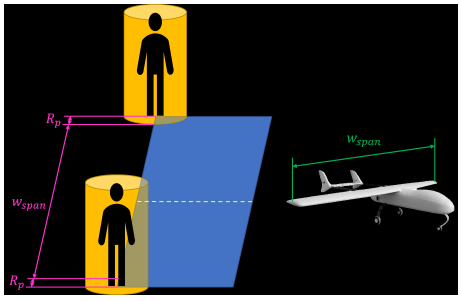


Fig. 4 Width of the area affected by the fall of the fixed-wing aircraft.

After assessing the size of the affected area, the population density of the affected area ρ_{people} needs to be precisely determined. According to Ref [24] and Ref [25], to protect the privacy, the government population data is aggregated and therefore not available at building level. However, in order to accurately estimate the risk of an aircraft to pedestrians in a particular area of the ground, we still need to estimate population density information at the building level.

According to Ref [26] and Ref [27], dasymetric mapping (also referred to asdasymetric modeling) is a technique where additional data (called ancillary data) is employed to guide the redistribution of populationdata at a finer level of

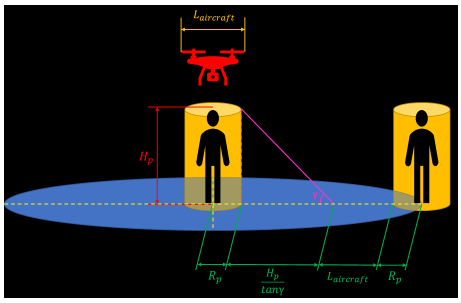


Fig. 5 Radius of the area affected by the fall of the rotor aircraft.

resolution. Initially, Eicher and Brewer proposed a simple dasymetric mapping method called binary mapping. Binary mapping subdivids zones into populated and unpopulated areas. In populated areas the areal weighting method is applied [28]. However, this method relies on the assumption that the population is uniformly distributed within the populated areas which is its main drawback [29].

In order to solve the above problem and to estimate the population distribution more accurately, the multi-class dasymetric mapping method came into being. The territory is partitioned into several residential classes (e.g., high density, medium density,low density) associated with different population densities [28].

As mentioned above, the study area is divided into eight parts using the MODUM method. In order to ensure the accurate estimation of population distribution while keeping the calculation simple, this paper adopts the multi-class dasymetric mapping method. It is based on the assumption that population is evenly distributed within an area covered by the same residential class.

Based on the previous studies, empirical analysis finds a strong positive correlation between population density and two subjective-criteria measures of quality of life [30]. To this end, combined with the MODUM area division method and the close relationship between population density distribution and area function, referring to the multi-class dasymetric map method, the population weights are allocated according to the functions of different areas, and a distribution map of population density is generated. The distribution of population density weights is shown in Table 1. The distribution ratio of weights refers to the polygon three-class method (P2) in Ref [28]. After obtaining the average population density of the study area and the population distribution weight of each part in the area, the population density ρ_{people} of each part can be obtained.

Table 1 Distribution of population density weights.

Area type	weight
None	0
High Street and Promenades	0.05
Railway Buzz	0.05
Waterside Settings	0.05
Countryside Sceneries	0.075
Suburban Landscapes	0.075
The Old Town	0.2
Victorian Terraces	0.2
Central Business District	0.3

After evaluating the number of pedestrians affected N_{people}, the fatality rate of aircraft to pedestrians $P_{peoplefatality}$ is calculated by equation 33.

$$P_{peoplefatality} = \frac{1}{1 + \sqrt{\frac{\alpha}{\beta}} \left(\frac{\beta}{E_k}\right)^{\frac{1}{4c_{shelter}}}} \tag{33}$$

When estimating the impact of an aircraft fall on pedestrians on the ground, it is necessary to consider the sheltering effect of buildings and trees on the impact. The shelter factor defines the shelter level of the map. The shelter factor is a positive number used to quantify the shelter level of people in the area. This is very important to consider, because the presence of buildings and other obstacles in the aircraft crash area can reduce the kinetic energy at the time of impact, thereby reducing the probability of death. If shelter factors are not evaluated, the resulting risks may be too conservative, especially in urban environments where buildings, vehicles, and trees protect the population. The value of the shelter factor $c_{shelter}$ is shown in the Table 2. Shelter factor varies with zone type.

Table 2 Value of the shelter factor.

Shelter type	$c_{shelter}$
None	1
High Street and Promenades	0.8
Railway Buzz	0.75
Waterside Settings	0.7
Roads	0.5
Countryside Sceneries	0.5
Suburban Landscapes	0.45
The Old Town	0.35
Victorian Terraces	0.3
Central Business District	0.25

IV. Case study

In this section, we simulate a mission scenario where a courier multi-rotor drone takes off from Cranfield University Airport to deliver packages to the VTOL airport at the train station in the city centre of Milton Keynes. The study area is selected as the town Milton Keynes near Cranfield University, and the area is a rectangular area about 20 km long and 15 km wide, as shown in figure 6. We use the proposed approach to perform the risk assessment for this specific case study as an illustrative example.



Fig. 6 Research area of the case study.

A. Risk assessment modelling

Using the road information KML file downloaded online from the overpass-turbo road information website [31], the risk assessment of the road information is carried out. The urban functional area distribution data and population

distribution data are obtained from Consumer Data Research Center (CDRC). It is a typology of neighbourhoods based on a number of built environment and urban morphology attributes, such as street / railway network, green spaces, retail access and historic buildings. The obtained original mature area division data is shown in Figure 7.

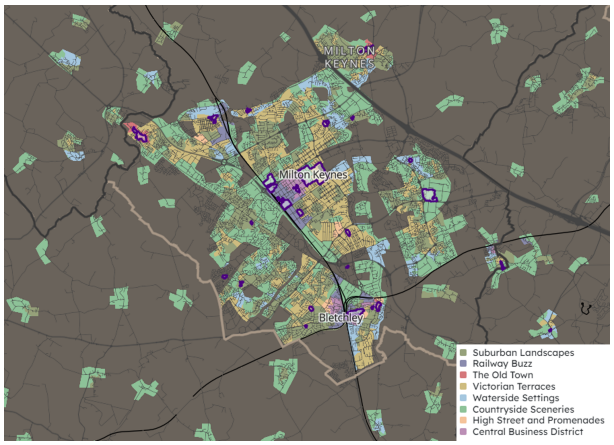


Fig. 7 Population distribution data of the area from CDRC.

The aircraft type is selected as rotorcraft for package delivery. The specific parameters of the aircraft are shown in Table 3.

Table 3 Aircraft performance parameters.

Aircraft mass m	1.4 kg
Cruising speed v_{cruise}	6.5 m/s
Cruising altitude H	50 m
Vertical windward area A	0.02 m^2
Horizontal windward area $A_{horizontal}$	0.15 m^2
Drag coefficient C_D	0.45

B. Risk cost map generation

Combined with the above mentioned risk assessment considerations, road and pedestrian risk assessment programs are developed. Using the Python programs, the road and pedestrian risk cost distribution in the form of KML are generated. The road risk cost map, pedestrian risk cost map and comprehensive risk cost map are displayed in GoogleEarth Pro. The processing flow of the programs is shown in Figure 8.

1. Generation of road traffic risk cost map

The final road risk cost distribution map is shown in Figure 9a. The red arrow represents the wind direction at that time, and the yellow path is the road in the map. Road types are divided into motorway, trunk, primary, secondary. The rainbow trajectory in the figure represents the distribution of road risk costs. The rainbow bars on the right represent the colors corresponding to the cost of risk. As the cost of risk value goes from high to low, the color of the trajectory gradually changes from red to green. It should be noted that the road risk cost distribution is not directly above the road, because of the impact of wind.

2. Generation of pedestrian risk cost map

The pedestrian risk cost distribution map is shown in Figure 9b. The red arrow represents the wind direction at that time and the rainbow bars on the right represent the colors corresponding to the cost of risk.

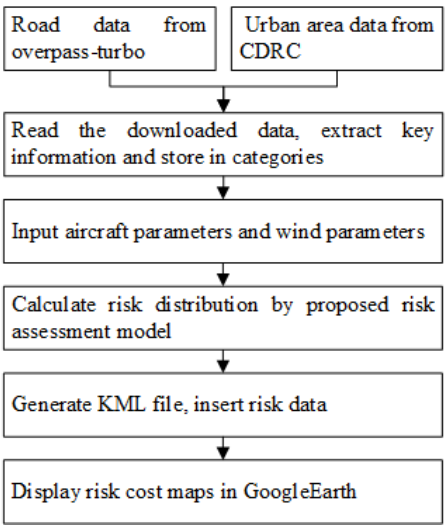
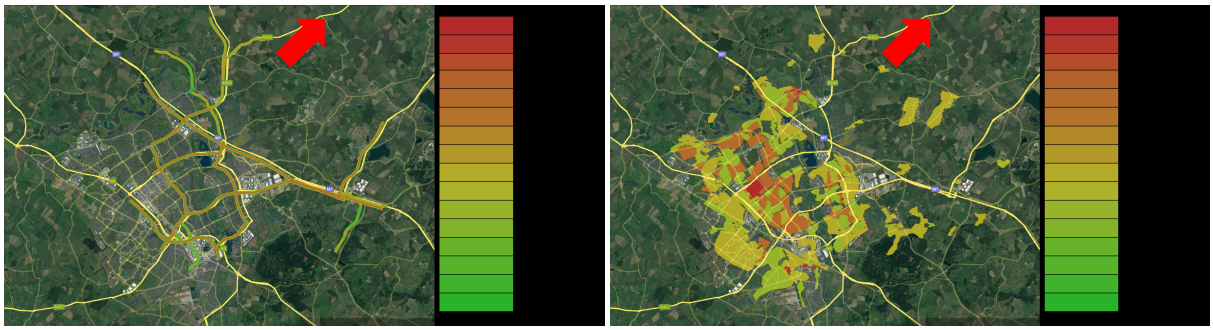


Fig. 8 Flow chart of the risk assessment program working process.



(a) Road traffic (b) Pedestrian

Fig. 9 Generated risk cost distribution map.

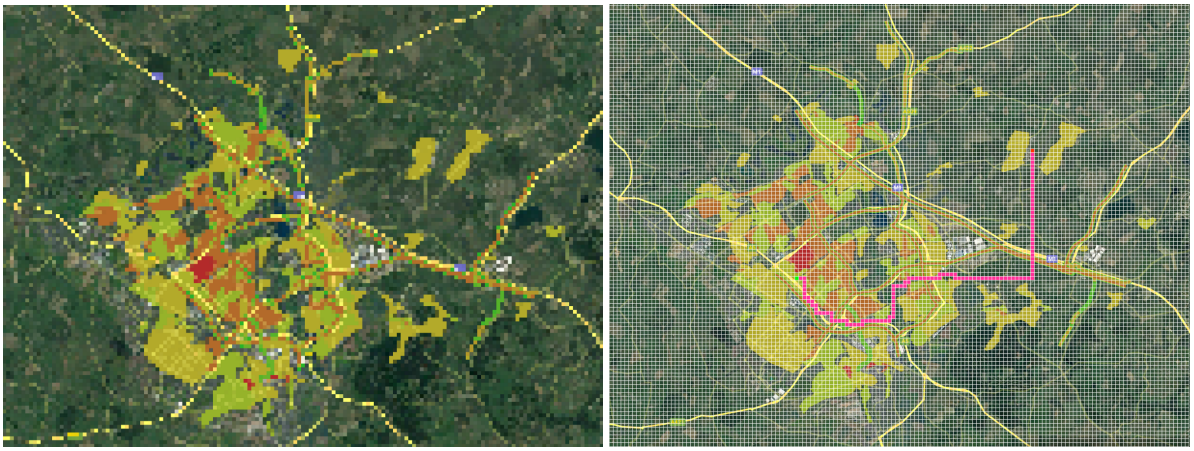
C. Mitigation recommendation

After the risk cost distribution map for roads and pedestrians is generated, We put the road risk weight and the pedestrian risk weight in a one-to-two ratio, and superimpose the two to form the total risk. And generate a comprehensive risk-cost distribution map of the area. A low-risk flight plan can be generated based on the comprehensive risk cost distribution in combination with the path planning algorithm. To deploy the path planning algorithm, the rectangular study area is first gridded. Each cell is a square with a side length of 100m. The risk cost distribution map after gridding is shown in Figure 10a.

The path planning process adopts the A* algorithm. The algorithm heuristic function uses Manhattan distance, and the weight of a node is the risk value of the area occupied by the cell. The final low-risk flight path planned according to the risk cost map is shown in Figure 10b. The green cell in the figure represents the end point of the flight path, the red cell represents the start point of the flight path, and the pink path is the low-risk flight path planned by the A* algorithm.

V. Conclusions and future work

In this paper, a pre-flight risk assessment framework has been proposed for UAM operations in future urban environment. The framework can quantitatively assess the risk value and produce the cost distribution to ground vehicles and pedestrians for fixed-wing aircraft and rotorcraft respectively. According to the proposed risk assessment framework, a specific real world urban area is selected, and the pre-flight risk assessment and flight plan formulation considering the risk are carried out by taking the UAS urban cargo transportation service as a case study. Finally, the



(a) Gridded risk cost map (b) Low-risk flight plan

Fig. 10 Flight mission planning based on the comprehensive risk cost map.

obtained risk cost map is gridded and processed by the A* path planning algorithm to generate a low-risk flight plan.

Future work will further improve and complement the proposed risk assessment framework, including the descent model of tilt-rotor aircraft and aircraft with parachutes, etc. Future work will also consider other sources of risks, both from aerial and ground, to perform a comprehensive risk assessment of UAM flights. This may include adding the risk assessment of other UAM participants located in urban mission airspace as well as civil aviation passing through the airspace.

Also, the flight plan generation approach based on risk cost map will also be optimized. When the risk cost map is gridded, the quadtree map and other methods will be introduced to compress the map capacity to reduce the computational burden of the path planning algorithm. In addition, different path planning algorithms and optimization directions will be considered to generate different flight paths such as the shortest distance flight path within the risk threshold, the lowest pedestrian risk path, the lowest vehicle risk path, etc., so as to provide the most suitable option according to the type of the mission.

References

[1] Reshma, R., Ramesh, T., and Sathishkumar, P., "Security situational aware intelligent road traffic monitoring using UAVs," *2016 international conference on VLSI systems, architectures, technology and applications (VLSI-SATA)*, IEEE, 2016, pp. 1–6.

[2] Kopardekar, P., "Urban Air Mobility Regional Readiness," Tech. rep., 2019.

[3] Menouar, H., Guvenc, I., Akkaya, K., Uluagac, A. S., Kadri, A., and Tuncer, A., "UAV-enabled intelligent transportation systems for the smart city: Applications and challenges," *IEEE Communications Magazine*, Vol. 55, No. 3, 2017, pp. 22–28.

[4] Qi, F., Zhu, X., Mang, G., Kadoch, M., and Li, W., "UAV network and IoT in the sky for future smart cities," *IEEE Network*, Vol. 33, No. 2, 2019, pp. 96–101.

[5] Kopardekar, P., Rios, J., Prevot, T., Johnson, M., Jung, J., and Robinson, J. E., "Unmanned aircraft system traffic management (UTM) concept of operations," *16th AIAA Aviation Technology, Integration, and Operations Conference*, AIAA, 2016, pp. 1–16.

[6] Murzilli, L., "JARUS guidelines on Specific Operations Risk Assessment (SORA)," , 2017.

[7] Capitán, C., Capitán, J., Castano, A. R., and Ollero, A., "Risk Assessment based on SORA Methodology for a UAS Media Production Application," *2019 International Conference on Unmanned Aircraft Systems (ICUAS)*, IEEE, 2019, pp. 451–459.

[8] Murzilli, L., et al., "JARUS guidelines on specific operations risk assessment (SORA), Public Release Edition 2.0, Joint Authorities for Rulemaking of Unmanned Systems," , 2020.

[9] Primatesta, S., Guglieri, G., and Rizzo, A., "A risk-aware path planning strategy for UAVs in urban environments," *Journal of Intelligent & Robotic Systems*, Vol. 95, No. 2, 2019, pp. 629–643.

[10] Primatesta, S., Rizzo, A., and la Cour-Harbo, A., "Ground risk map for unmanned aircraft in urban environments," *Journal of Intelligent & Robotic Systems*, Vol. 97, No. 3, 2020, pp. 489–509.

[11] Wu, P. P.-Y., Campbell, D., and Merz, T., "Multi-objective four-dimensional vehicle motion planning in large dynamic environments," *IEEE Transactions on Systems, Man, and Cybernetics, Part B (Cybernetics)*, Vol. 41, No. 3, 2010, pp. 621–634.

[12] Bertrand, S., Raballand, N., Viguier, F., and Muller, F., "Ground risk assessment for long-range inspection missions of railways by UAVs," *2017 International Conference on Unmanned Aircraft Systems (ICUAS)*, IEEE, 2017, pp. 1343–1351.

[13] Bertrand, S., Raballand, N., and Viguier, F., "Evaluating ground risk for road networks induced by uav operations," *2018 International Conference on Unmanned Aircraft Systems (ICUAS)*, IEEE, 2018, pp. 168–176.

[14] Zhou, Q., and Xu, M., "Research On Risk Assessment Of UAV To Buildings," *2021 International Conference on Information Control, Electrical Engineering and Rail Transit (ICEERT)*, IEEE, 2021, pp. 37–40.

[15] Xinting, H., and Fuqing, D., "Risk assessment model for UAV operation considering safety of ground pedestrians in urban areas," *China Safety Science Journal*, Vol. 30, No. 8, 2020, p. 137.

[16] AMU-LED, "D2.2.010 High Level ConOps - Initial," Tech. Rep. Edition 00.01.00, SESAR JU, 2021.

[17] Hu, X., Pang, B., Dai, F., and Low, K. H., "Risk assessment model for UAV cost-effective path planning in urban environments," *IEEE Access*, Vol. 8, 2020, pp. 150162–150173.

[18] Petritoli, E., Leccese, F., and Ciani, L., "Reliability and maintenance analysis of unmanned aerial vehicles," *Sensors*, Vol. 18, No. 9, 2018, p. 3171.

[19] la Cour-Harbo, A., "Quantifying risk of ground impact fatalities for small unmanned aircraft," *Journal of Intelligent & Robotic Systems*, Vol. 93, No. 1, 2019, pp. 367–384.

[20] Dalamagkidis, K., Valavanis, K. P., and Piegl, L. A., "Evaluating the risk of unmanned aircraft ground impacts," *2008 16th mediterranean conference on control and automation*, IEEE, 2008, pp. 709–716.

[21] Bleier, M., Settele, F., Krauss, M., Knoll, A., and Schilling, K., "Risk assessment of flight paths for automatic emergency parachute deployment in UAVs," *IFAC-PapersOnLine*, Vol. 48, No. 9, 2015, pp. 180–185.

[22] Clothier, R., Palmer, J., Walker, R., and Fulton, N., "Definition of airworthiness categories for civil Unmanned Aircraft Systems (UAS)," *Proceedings of the 27th Congress of the International Council of the Aeronautical Sciences*, Optimage Ltd. on behalf of the International Council of the Aeronautical . . . , 2010, pp. 1–12.

[23] Lum, C., and Waggoner, B., "A risk based paradigm and model for unmanned aerial systems in the national airspace," *Infotech@ Aerospace 2011*, 2011, p. 1424.

[24] Ural, S., Hussain, E., and Shan, J., "Building population mapping with aerial imagery and GIS data," *International Journal of Applied Earth Observation and Geoinformation*, Vol. 13, No. 6, 2011, pp. 841–852.

[25] Sridharan, H., and Qiu, F., "A spatially disaggregated areal interpolation model using light detection and ranging-derived building volumes," *Geographical Analysis*, Vol. 45, No. 3, 2013, pp. 238–258.

[26] Semenov-Tian-Shansky, B., "Russia: Territory and population: A perspective on the 1926 Census," *Geographical Review*, 1928, pp. 616–640.

[27] Wright, J. K., "A method of mapping densities of population: With Cape Cod as an example," *Geographical Review*, Vol. 26, No. 1, 1936, pp. 103–110.

[28] Eicher, C. L., and Brewer, C. A., "Dasymetric mapping and areal interpolation: Implementation and evaluation," *Cartography and Geographic Information Science*, Vol. 28, No. 2, 2001, pp. 125–138.

[29] Maantay, J. A., Maroko, A. R., and Herrmann, C., "Mapping population distribution in the urban environment: The cadastral-based expert dasymetric system (CEDS)," *Cartography and Geographic Information Science*, Vol. 34, No. 2, 2007, pp. 77–102.

[30] Rappaport, J., "Consumption amenities and city population density," *Regional Science and Urban Economics*, Vol. 38, No. 6, 2008, pp. 533–552.

[31] Olbricht, R., "Overpass-turbo," `https://overpass-turbo.eu/`, 2022. Accessed 2011.



https://dspace.org/

Risk-based flight planning and management for urban air mobility

Su, Yu; Xu, Yan

2022-06-20
AIAA
https://doi.org/10.2514/6.2022-3619
Su Y, Xu Y. (2022) Risk-based flight planning and management for urban air mobility. In: AIAA Aviation 2022 Forum, 27 June - 1 July 2022 Chicago, IL, Article number AIAA 2022-3619

Downloaded from a DSpace repository. https://dspace.org/